Recovery of technologically critical lanthanides from ion adsorption soils

DOI:
10.1016/j.mineng.2021.106921

Document Version
Accepted author manuscript

Recovery of technologically critical lanthanides from ion adsorption soils

Anthony Stockdale [a, b, 1], Steven A. Banwart[b]

[a]Department of Earth and Environmental Sciences, The University of Manchester, Manchester, M13 9PL, United Kingdom

[b]School of Earth and Environment, University of Leeds, Leeds, LS2 9JT, United Kingdom.

[1]Corresponding author E-mail: tony@biogeochemistry.org.uk

VERSION – This is the accepted version of the manuscript prior to final production. The definitive version of the manuscript is available from the publisher at https://dx.doi.org/10.1016/j.mineng.2021.106921

Abstract

Rare earth elements (REEs) are in increasing demand due to rapidly rising use in consumer technology, the automotive industry and in renewable energy generation systems, amongst other technology sectors. Ion-adsorption type REE ore deposits are currently being exploited in China's southern provinces and there is increasing interest in identifying potential reserves globally. Here we investigated the extraction of REEs from an ion-adsorption clay sampled at a surficial deposit in Madagascar. Using a 1 M NH_4Cl lixiviant salt solution, chosen based on experimental evidence to maximise REE extraction, minimises undesirable dissolved Al in eluate. Lower Al concentration in solution reduces its interference with NH_4^+ in oxalate precipitation of REEs in the extraction process. We show that NH_4Cl solutions can be used to efficiently extract REE with relatively low lixivient volumes in a through-flow column system. We show that when extraction with a pulse of lixiviant is followed by a rinsing step, there are several identifiable stages during the extraction process, including a marked increase in total lanthanides extracted, which is correlated with the breakthrough of ammonium ions, and where the eluted dissolved Al concentration decreases from its peak concentration.

Keywords: rare earth elements; lanthanides; technologically critical elements; lixiviant; ion-adsorption deposits

1. Introduction

Rare earth elements (REEs; Y, Sc and lanthanide elements) are increasingly in demand due to rapidly rising use in consumer technology, the automotive industry and in renewable energy generation systems, amongst other technology sectors (Chakhmouradian and Wall, 2012). A significant majority of the world's REE supply comes from China, with Bayan Obo (Inner Mongolia) one of the largest deposits (Kynicky et al., 2012). In 2019 significant mine production was also undertaken in Myanmar, USA and Australia (10-12% of total mine production); with Brazil, Vietnam and Russia estimated to have significant reserves (10-18% of the global total) but representing only 0.4-1.3% of total production (USGS, 2020).

The majority of REE metals are mined from open pits of bastnasite and/or monazite. A smaller fraction is extracted from leaching of surficial deposits of ion-adsorption clays (Vahidi et al., 2016). Grades within bastnasite and monazite deposits can be as high as 8%, whereas ion-adsorption type rare earths ore are typically 0.02%–0.5% as weight percent of rare earth oxides (Kanazawa and Kamitani, 2006; Moldoveanu and Papangelakis, 2013b). However, ion-adsorption deposits can contain a much higher proportion of higher value heavy REEs. Life Cycle Assessments have concluded that these deposits result in lower environmental impacts due to lower energy requirements for mining and extraction compared to other sources when an economic value-based allocation is used (Vahidi et al., 2016). Current exploitation of these deposits is being conducted in China's southern provinces (Kanazawa and Kamitani, 2006).

In situ leaching of ion-adsorption deposits involves direct injection of an extraction lixiviant solution (typically $(NH_4)_2SO_4$) into the orebody via a leaching hole. Typically at a depth of 1.5-3 m, generally above the water table, diameter of 0.8 m in an array 2-3 m apart that can span up to 100 m across. The lixiviant solution is injected at high pressure and flows through the pores of the orebody and is either pumped above-ground through the recovery wells, or collected in sumps at the water table surface. The loaded leach solution is pumped above-ground for further processing, with the maximum possible REE extraction taking up to 400 days, primarily controlled by the residence time of injected fluids during largely vertical downward flow to the collection wells (Moldoveanu and Papangelakis, 2016). A feature of recovery from these deposits is fast extraction kinetics (minutes for terminal extraction), instantaneous compared to transport time scales of extracted metals, and is independent of lixiviant concentration (above a threshold value related to the ion exchange capacity of the ore) and pH. Elevated temperatures do not increase extraction efficiency but have a positive

effect on extraction time (Xiao et al., 2015). However, establishing temperatures above ambient within an ore body will be technically difficult and add to energy demands and engineering costs with only small potential gains in metal extraction.

For downstream processing, loaded lixiviant solutions are generally put through a lanthanide precipitation procedure as an initial concentration step before further processing of the concentrated solids. Examples of uses of oxalate precipitation as part of lanthanide recovery processes can be found in Fernandes et al., 2013; and Josso et al., 2018, presenting recovery from environmental deposits and battery recycling, respectively.

The increase in demand for REEs has led to a greater focus on security of supply by many national governments and this has fuelled interest is assessment of previously unexploited international ion-adsorption deposits. Recent studies have assessed deposits in the Philippines (Padrones et al., 2017), Madagascar (SRK Exploration Services Ltd, 2013), Malawi (Le Couteur, 2011), Brazil (Rocha et al., 2013), Laos (Sanematsu et al., 2009) and Vietnam (Mentani et al., 2010). Further studies have also investigated the efficacy of compound leaching (using combinations of dissolved salts), which aims to either improve extraction efficiency, reduce interference of REE concentration by Al, or reduce the environmental impact of lixiviant solutions (e.g., Yang and Zhang, 2015; He et al., 2016; and Xiao et al., 2017). Bioleaching has also been investigated with the aim of providing an economically and environmentally viable alternative to current approaches (Barnett et al., 2018).

Several prior studies have presented data on the optimum lixiviant composition and its concentration as well as reaction conditions (e.g., pH and temperature). To date there are few investigations that present high resolution data on REE extraction that are obtained under reactions conditions that potentially replicate those within an ore body. In particular, covering conditions that represent a more complete processing stream of the lixiviant injection, extraction and washing phases. The primary aim of this work was to investigate, at high temporal resolution at laboratory bench scale, processes occurring when lixiviants are pumped through ion-adsorption soils, simulating in situ extraction (using packed columns). In addition we sought to investigate some of the soil properties, the effects of lixiviant cations and anions on extraction efficiencies and to perform a preliminary investigation on the potential

interference of lixiviant cations on the precipitation of lanthanide oxalate salts by formation of lixiviant cation-oxalate precipitates.

2. Methods

Our experimental design was planned as an analogue to the process stream of extraction, recovery and washing of REEs from ion adsorption clays. Batch desorption studies investigated lixiviant extraction efficiency, column studies identified lixiviant volume requirements and oxalate precipitation studies identified interference from lixiviant cations. Results were used to select conditions for further high temporal resolution column experiments. In addition, we characterised several soil properties relevant to in situ extraction of REEs. Descriptions of the main methods are included below, detailed methods are included in the Supporting Information (SI) Section S2.

2.1 Source of soil samples

Ion-adsorption soils were obtained from a deposit located in the Cenozoic Ambohimirahavavy alkaline complex in northern Madagascar, conducted as part of the UK Natural Environment Research Council project SoS RARE (NE/M011232/2). The mineralized lateritic regolith being derived from the weathering of alkaline igneous rocks (Estrade et al., 2019; see also a comprehensive characterisation of the same region in SRK, 2008; and Stoltz, 2017; these include; lithology structures and regolith of the local geology; parent ion-adsorption mineral characterisation using quantitative evaluation of minerals by scanning electron microscopy, XRF and XRD; REE sequential extractions; as well as airborne geophysical surveys and outcrop sampling). A subset of 6 bulk samples were chosen for analysis here, to represent the range of pit locations, depths and soil properties. Sample 0547 was used for a significant number of experiments due to it representing a large depth horizon and falling in the middle of the range of total lanthanide concentrations of soils across the site (Estrade et al., 2019).

2.2. Soil properties and preparation

Analyses were performed to determine mineral composition, BET surface area, particle size distribution and complexed-copper-method cation exchange capacity (full methods described in SI Section 2.1). For batch and column experiments the soil samples were air-dried and sieved through a 1.4 mm mesh to remove large mineral fragments. The remaining soil was

gently disaggregated in a pestle and mortar until all of the sample passed through a 250 μm sieve. Any further processing for supplementary experiments is detailed in the SI.

2.3. Experimental procedures

2.3.1. Batch experiments. These tested the efficiency of various lixiviant solutions containing different cations (H^+, NH_4^+, Ca^{2+}, Mg^{2+}) and anions (ClO_4^-, Cl^-, NO_3^-, SO_4^{2-}). SI Table S2.1. details the range of reagents used for the experiments. Lixiviants of monovalent salts were 1 M, those of salts containing divalent cations or anions were 0.5 M (consistent with good extraction rates in lixiviants of 0.5 M or greater as determined by Moldoveanu and Papangelakis, 2013). To a 1 g sample of soil 0547 in a micro-centrifuge tube was added 1 mL of solution, thorough mixing was achieved with a vortex mixer. Each solution experiment was performed in triplicate. After 24 hours the slurries were centrifuged (micro-centrifuge 13'200 rpm, 5 minutes). Each centrifugate was filtered (Whatman Puradisc polyethersulfone 0.45 μm syringe filter, 13 mm), before pH and conductivity analysis of the supernatant (SI Table S2.2.). Filtered fluid samples were stored refrigerated in micro-centrifuge tubes awaiting appropriate dilution/acidification for ICP analysis.

2.3.2. Through-flow column experiments. Soil through-flow experiments were performed using chromatography columns (Omnifit EZ-AA 25mm/400mm) with an internal diameter of 25 mm and two adjustable end-pieces fitted with 5 μm pore PTFE frits. Columns were pre-conditioned by circulating, in a closed loop, a small volume (< 300 mL) of MQ water for >7 days (See SI.2.1.5. for filling and conditioning procedure used). Filled conditioned columns were connected to a peristaltic pump tube (Tygon S3™ E-LFL, 0.1 or 0.06 mL min^{-1} flow rate) clamped onto a fixed flow rate pump (Bran Luebbe). Flow rate was ultimately governed by the balance of the input pressure and hydraulic pressure in the column (see the SI Table S2.3. for the approximate flow rates achieved in each of the column experiments). Preliminary experiments were performed on the more coarsely grained and presumably more permeable 0652 sample to test the system with lower hydraulic pressures and to gain insight into the pore volumes of lixiviant required for extracted metal breakthrough. The systems were then switched to the finer grained 0547 sample, where a low pore volume of lixiviant was passed through the column before switching to a post-lixiviant low ionic strength solution. Small variances were made with lixiviant pH for different columns to determine any effect of this lixiviant property (details in SI Table S.2.4.).

***2.3.3. Oxalate precipitation experiments*.** We investigated the potential for different lixiviant cations to interfere with the precipitation of lanthanide oxalates, on the basis that this is a typical initial concentration step in some industrial extraction process streams (ammonium bicarbonate is also used; Vahidi et al., 2016; Chi et al., 2003). To obtain a loaded lixiviant solution 50 g of soil 0547 was added to 500 mL of each of four salt solutions (1 M NH_4Cl, NaCl, $MgCl_2$, $CaCl_2$). The resultant slurries were shaken on a table shaker for ~3 days then left to stand for several weeks. The slurries were then centrifuged and the supernatant filtered (0.45 μm polyethersulfone, Sartorius Minisart) and analysed for total dissolved concentration of lanthanide elements (reported in SI.2.1.4). To triplicate 50 mL subsamples of each loaded solution was added 50 mL of 0.6 M oxalic acid (Aldrich, purified grade ≥99.999% trace metal basis). At several time intervals, up to 21 days, 1 mL subsamples were filtered (Whatman Puradisc polyethersulfone 0.45 μm syringe filter, 13 mm) and immediately diluted 10-fold and acidified with 200 μL of HCl (Honeywell-Fluka, ACS Reagent, ≥37%). This avoided further precipitation of oxalate salts whilst solutions were awaiting analysis for total dissolved lanthanide element concentrations.

***2.3.4. Chemical analysis of solutions*.** Dissolved metals (Al and lanthanides) were analysed using a Thermo Fisher iCAPQc or X-Series 2 ICP-MS following suitable dilution. Conductivity and pH were measured with a Mettler Toledo Seven Excellence meter coupled to a pre-calibrated conductivity probe InLab 752-6mm using a VWR Prolab 50000 μS/cm standard (25°C, KCl) as a quality control, and a InLab Micro Pro-ISM pH electrode calibrated on the hydrogen ion activity scale with three National Institute of Standards and Technology traceable standard buffers (pH 4.00, pH 7.00, and pH 10.00). Typical detection limits were 1.7, 9.7, 5.5, 2.3, 6.1, 0.4, 0.4, 0.8, 0.4, 0.7, 0.4, 0.5, 0.4, 0.4 and 0.5 for Al, La, Ce, Pr, Nd, Sm, Eu, Gd, Tb, Dy, Ho, Er, Tm, Lu and Yb respectively, units nmol L^{-1} except Al as μmol L^{-1}.

2.4. Geochemical modelling of experimental systems

We compare the Al concentration data from column studies to the theoretical solubility of gibbsite and kaolinite at equilibrium with the ionic composition appropriate matrix at 293 °K. Modelling of solution and solid phase thermodynamic equilibria used the geochemical modelling code PHREEQC (Parkhurst and Appelo, 2013), with the Lawrence Livermore National Laboratory database (reviewed in Meeussen et al, 2009).

3. Results

3.1. Soil properties

The soil samples are predominantly kaolinite, with lower quantities of gibbsite and quartz. Surface area (SA) and cation exchange capacity (CEC) analysis showed that the visually coarser sample (0652) had the lowest values (SA 33.7 $m^2\ g^{-1}$; CEC 3.7 meq 100 g^{-1}) with the sample used for the batch and second phase of column experiments (0457) having the highest values (SA 49.6 $m^2\ g^{-1}$; CEC 7.1 meq 100 g^{-1}). Mineralogy does not significantly differ with size fraction, except manganese oxide, which is present in greater quantities in the larger size fractions (detailed results for soil properties are reported in SI3.1.).

3.2. Extraction efficiency with cation and anions in lixiviant

The general pattern in quantity of lanthanide recovery with lixiviant cation is $NH_4^+ \approx Mg^{2+} \approx Ca^{2+} > H^+ > Na^+$. For anions the sequence is $SO_4^{2-} > NO_3^- > Cl^-, ClO_4^-$. However, where the cation is NH_4^+, Mg^{2+} or Ca^{2+} then high extraction rates are achieved and the counter-anion has no additional effect. Figure 1 shows these trends, for total lanthanides, plotted against the Gibbs free energy of solvation for the cations (other than ammonium). Less negative solvation energy cations have lower total lanthanide extraction than more negative solvation energy cations. Data for each individual lanthanide metal are shown in SI Figure S3.1.

The concentrations of co-extracted Al may affect the downstream lanthanide processing and is therefore an important factor in choosing a lixiviant. The general pattern in recovery of Al with different lixiviant cations follows the sequence $H^+ >> NH_4^+ > Mg^{2+} \approx Ca^{2+} > Na^+$. For anions the trend was $SO_4^{2-} > NO_3^- \approx ClO_4^- \approx Cl^-$ (Figure 2).

3.3. Oxalate precipitation of lanthanides in different matrices

Oxalic acid was added to lixiviant solutions loaded with dissolved lanthanide ions (using chloride salts for all solutions) prepared from soil 0547. In the presence of the Ca^{2+} lixiviant there was immediate precipitation of significant quantities of Ca oxalate with simultaneous precipitation of lanthanides (>99%). Mg and Na lixiviants resulted in formation of some visible

Mg or Na oxalate salts but there was minimal precipitation of lanthanides after a 21 day period (<5%). The NH_4Cl lixiviant resulted in no visible ammonium oxalate precipitation and approximately 50% of the total lanthanides were precipitated from solution under the experimental conditions (SI Figure S3.2.). Precipitation was not equal for all lanthanides, Sm and Eu were the most depleted from solution with ~75% precipitated after 21 days. Lighter and heavier elements then progressively had lower levels of precipitation, with La, Er, Tm, Yb and Lu having >60% remaining in solution after 21 days (SI Figure S3.3.).

3.4. Extraction in lixiviant through-flow systems

Scoping experiments on the 0652 soil showed that the extraction of a large proportion (~80%) of the lanthanides was realised after <0.3 pore volumes of lixiviant solution had eluted from the column (Figure 3 and SI Figures S3.4., S3.5.), with breakthrough occurring at 1.3-1.4 pore-volumes and the rapid desorption phase completed at 1.5-1.6 pore volumes. Further contact with lixiviant resulted in limited further recovery, with <95% recovery with 12 pore volumes. Results show that more than one pore volume of fluid is required to be passed through the column before breakthrough of the lixiviant. This may be due to a combination of exchange with inner pore waters, changes to the column packing properties after lixiviant injection, and/or dead volumes in column input and output tubing. The typical profile of extraction in each lixiviant fraction is shown in SI Figure S3.6., for each individual lanthanide. Only lanthanum shows deviation in the extraction behaviour compared to other metals, with a steeper initial breakthrough curve. A final bulk ion-exchange leach using $CaCl_2$ (performed in a batch reaction on solids recovered from the column after approximately 8-12 pore volumes of lixiviant through-flow) yielded 9-14% of the total La or Ce and 1-6% of other lanthanides. The addition of acid to the $CaCl_2$ leach slurries reveals that some lanthanides are present at significant concentrations only as acid-extractable forms (SI Table S3.6.). Acid extracted Ce is 67% of the ion-exchangeable mass of Ce; Gd, Tm, Yb and Lu are 20, 22, 36 and 32%; with other acid extracted metallic elements at lower amounts (5-17% of the ion-exchangeable).

Informed by the scoping experiments, further through-flow experiments on sample 0547 used 1 M NH_4Cl as the lixiviant, low lixiviant volumes (<0.5 pore volumes) and were followed by a rinse solution (0.05 M NaCl or MQ water; informed by previous work revealing water content trapped in leached material contained significant amounts of REE and residual lixiviant that required thorough washing of the solid residue (Moldoveanu and Papangelakis, 2016)). In replicate columns >95% of the ion-exchangeable lanthanides are extracted with the small

lixiviant injections (Figure 3 lower panel and SI Figures S3.4., S3.5). The final bulk ion-exchange leaches yielded 1-6% of the total ion-exchangeable fraction for the lanthanide metals. The addition of acid to the $CaCl_2$ leach slurries resulted in extraction of 24% more Ce and 3-11% of the ion-exchangeable for other metals (SI Table S3.6.). Figure 4 details the lixivient analyte, pH, Al, and total lanthanide breakthrough curves for a typical column experiment (the same experiment as Sample 0547, Column E in Figure 3). Chloride as the conservative tracer, breaks through at the same stage as the marked decrease in pH and increase in Al and lanthanides (for the breakthrough curves of other 0547 columns see SI Figure S3.7.). The sum of the ion-exchangeable Al, converted to equivalent units for cation exchange capacity, was 7.4 (± 1.5) meq 100 g^{-1}. The Al concentrations in the column eluent fractions (post Cl breakthrough and when the pH is lower than 4.5) tends to follow the theoretical solubility of Al oxide or hydroxide mineral phases in equilibrium with the matrix solution (SI Figure S3.8.). The dataset for the column experiments is publicly available (Stockdale and Banwart, 2021).

4. Discussion

We studied the extraction efficiency of lixiviants in terms of both cations and anions in the lixiviant salt solution. When compared with the Gibbs free energy of solvation, cations with less negative values have lower extraction efficiencies (Figure 1). Ammonium, together with the divalent cations with the more negative solvation energies, exhibit the most complete extraction. This is consistent with the proposed ion-exchange mechanism of Moldoveanu and Papangelakis (2012). Their model states that cations with low negative hydration enthalpies ($-\Delta H_{hyd}$), which are able to dehydrate completely at ambient temperature and reside directly on the clay surface, establish a strong electrostatic bond. In contrast to cations with high $-\Delta H_{hyd}$ (such as REEs) that remain partially hydrated and thus establish weaker bonds with the negative charge on the surface, thus making ion-exchange more energetically favourable for cations with high $-\Delta G_{solv}$ values.

The counter anions in the lixivient will affect desorption processes by shifting the equilibrium of the aqueous REE ion complexes by reducing the activity of the free aquo ion, and thus in turn, will result in some desorption from ion-adsorption sites in order to maintain aqueous speciation equilibrium between the exchange surface and the bulk solution. For example, the stability constants (log K, at 25 °C and ionic strength of 1) of the anions ClO_4^-, Cl^-, NO_3^- and SO_4^{2-} for equilibrium with Ce^{3+} are 0.15, -0.04, 0.2 and 1.51, respectively (Martell et al., 2004).

297 Therefore, in lixiviants where the efficiency (in terms of surface desorption) of the cation is not
298 maximised, the anion can have a positive effect on extraction efficacy and this is directly
299 related to the potential for the anion to form complexes with the REE metal ions (larger log Ks
300 results in higher aqueous concentrations of anion complexes with the target lanthanide metal
301 ion). This is seen in Figure 1 for Na, which has a relatively weak selectivity for ion adsorption
302 and therefore cation ion exchange and where the sulfate ion results in a greater REE
303 extraction than nitrate, chloride or perchlorate by reducing the solution free-ion activity of the
304 REE.

305

306 The shape of the Al eluate concentration profiles (Figure 4 and SI Figure S3.7) and the
307 relatively slow kinetics of kaolinite (Wieland and Stumm, 1992) and gibbsite (Bloom, 1983)
308 dissolution indicate that the high concentrations in the eluate solution occur as a result of
309 desorption from ion-exchange sites. Occupation of ion-exchange sites is dominated by Al^{3+} in
310 these systems, consistent with the conclusions of Crawford (2019) on samples from the same
311 region. Nevertheless, eluate dissolved Al concentrations closely follow those calculated from
312 the theoretical solubility of gibbsite in equilibrium with the eluate solution (Figure S3.8). The
313 level of Al extraction is an important consideration in the recovery of REEs, relative to the
314 target metals; Al is present in large quantities and not of economic interest. It may also interfere
315 with downstream refining and processing. The choice of lixiviant directly influences Al
316 extraction from the soil. Divalent cations and ammonium tend to maximise REE extraction,
317 irrespective of the lixiviant anion. Therefore, selection of the counter anion can be based on
318 the Al extraction rates and the amount of extracted dissolved Al is therefore minimised with
319 chloride salt solutions (Figure 2). This will be related to the level of speciation of Al with anion
320 ligands (stability constants (log K, at 25 °C and ionic strength of 1) of the anions Cl^-, and SO_4^{2-}
321 for equilibrium with Al^{3+} are −1.0 and 1.48, respectively; Martell et al., 2004). Sulfate species
322 in a 0.01 M $Al_2(SO_4)_3$ solution can represent 20% of total Al, in contrast to ~5% for nitrate
323 species in a $Al(NO_3)_3$ solution or <3% for perchlorate species in a $Al(ClO_4)_3$ solution (Urabe et
324 al., 2009). This is also consistent with the conclusions of Xiao et al. (2016), who reported lower
325 Al leaching in compound lixiviant mixtures (with sulfate and chloride salts) than with a sulfate
326 salt with the same cationic charge.

327

328 There are several methods developed for the recovery of REEs from aqueous solutions using
329 oxalate (e.g., Xia, 2018; Kasaini, 2015; and other patent applications cited therein). However,
330 this precipitation step is reliant on minimal interference from lixiviant cations. Dissolved ion

concentration at saturation with resect to oxalate salts follows the sequence NH_4 > Na >> Mg >> Ca (52, 36.1, 0.38 and 0.0061 g L^{-1} respectively; Lide, 2005) and our results indicated that in 1 M lixiviant solutions (0.5 M for Ca, Mg), the precipitation of lixiviant cation oxalate salts occurred for all cations except NH_4^+. Thus, where oxalate precipitation is used as a downstream processing step other lixiviant cations will be ineffective and the potential for use of compound lixiviants may also be constrained by the solubility of oxalate salts.

The patterns of precipitation of REE salts from loaded lixiviant solution after addition of oxalate follow a similar trend to that of Weaver (1954), who reported preferential precipitation of Sm, with lighter elements following in order of decreasing atomic number, and heavier elements following Sm in order of increasing atomic number. Here, we found the amount of Eu precipitated was slightly greater than that of Sm, and a slightly lower amount precipitated for Lu compared to that for Yb.

Experiments (on sample 0547) examined the breakthrough curve profiles of eluate chemistry under conditions where the soil is hydraulically saturated with fluid, followed by a relatively small pulse of lixiviant and then followed by a prolonged washing phase. The lixiviant used was NH_4Cl, optimised considering the results of previous experiments, i.e. to maintain high extraction efficiencies, to reduce the Al extraction and considering the need to use NH_4^+ to eliminate interference with oxalate precipitation. This is also consistent with the similar extraction efficiencies of $(NH_4)_2SO_4$ or NH_4Cl lixiviants as revealed from the work of Xiao et al. (2016).

Results from the scoping column experiments (on sample 0652) indicate that the number of pore volumes of lixiviant required for a high rate of REE extraction is low relative to the volume of soil. For sample 0547 in column experiments, 0.1 pore volumes of lixiviant will contain 3.2 ± 0.2 mmol of NH_4^+ per 100 g of soil, compared to a CEC of 7.1 meq 100 g^{-1}, suggesting that ~0.25 pore volumes of lixiviant will be sufficient for complete exchange of all sorbed ions, and this amount will be reduced where Al is not fully desorbed. We used ~0.4 (columns C, D and F) to 0.6 (column E) pore volumes of lixiviant (based on Cl in eluent), indicating that significant desorption can be achieved with lixiviant volumes around those required for saturation of ion-adsorption sites. Results are also consistent with the finding of other studies that indicate fast desorption kinetics (e.g., Moldoveanu and Papangelakis, 2012).

We identified several stages during lanthanide extraction in the column experiments (Figure S3.9.). In the first stage total La's (T-La) concentrations increase as Al increases and there is no ammonium breakthrough. In stage 2, Al reaches a peak breakthrough concentration but there are no significant change in T-La concentration. For stage 3, ammonium breakthrough occurs, Al concentration decreases from its peak value and there is a correlated increase in the amounts of T-La extracted. In the final phases Al and T-La concentrations both decrease as they are depleted from the column. Then, finally, the post-lixiviant wash results in a gradual decrease in the ammonium concentration.

Moldoveanu and Papangelakis (2013b) reported that there is a beneficial effect of batch leaching at lower pH, with slightly higher extraction levels being obtained at pH 3 versus pH 5 (86.5 vs. 82.1%). However, our column study indicates that pH variation of the lixiviant had little effect on the recovery efficiency of REE extraction. The equilibrium pH of freshly prepared 0.1 M NH_4Cl was 4.8 (columns C and E); two other columns (D and F) used solutions adjusted to pH 3 or 1. The pH changes in the column experiments during initial ion-exchange are driven by the hydrolysis of desorbed Al releasing protons ($Al^{3+} + H_2O = AlOH^{2+} + H^+$). Following Cl breakthrough, the pH in all columns was buffered to a value of ~3.2 irrespective of the input solution pH. To restore the soil to the original porewater pH required 1-1.5 pore volumes of flushing with low ionic strength solutions after lixiviant input. In columns with high throughputs of lixiviant (>7 pore volumes, columns A and B, using sample 0652), the pH initially drops but steadily increases towards the lixiviant equilibrium pH as the Al and REEs are desorbed from the soil.

Our results show that heavier REE metals and Ce have significant amounts present as acid extractable fractions that are not extracted by ion-exchange. For sample 0547 this phase represents >9% above the ion-exchangeable concentrations for Sm and heavier metals and 24% for Ce. For the coarser grained 0652 sample, this phase represents 13-36% for Sm and heavier metals and 67% for Ce. This is consistent with Estrade et al. (2019), who reported higher light REEs extraction rates from leaching than for heavy REEs for samples from the same deposit (from data based on more aggressive leaching procedures). Ce anomalies are a well understood feature of these deposits, related to the very low reduction potential of Ce(IV) to Ce(III) (Bard et a., 1985) promoting formation of cerianite (Moldoveanu and

Papangelakis, 2012). Reduction leaching has been investigated as a more efficient process for extraction of rare earth oxides (Xiao et al., 2016b).

5. Conclusions

The results of this study are of potential value to industry in terms of extraction optimisation and subsequent lowering of energy and lixiviant costs. Ammonium chloride appears to offer benefits as a lixivient over other salts with similar extraction efficiencies, as it minimises Al mobilisation and yields less contamination of recovered REE-oxalate mineral precipitates. We show that NH_4Cl solutions can be used to efficiently extract REE with relatively low lixivient volumes (compared to pore volumes) in a through-flow column system. The minimum relative volume required is likely related to the cation exchange capacity of the ore deposit, which will be closely associated with the exchangeable Al concentration.

Acknowledgements

Funding for this work was provided by the UK Natural Environment Research Council (NE/M011232/2). AS acknowledges support from the University of Manchester during the data analysis and manuscript preparation phases of this work.

References

Bard, A.J., Parsons, R., Jordan, J., 1985. Standard Potentials in Aqueous Solutions. Marcel Dekker, New York.

Barnett, M.J., Palumbo-Roe, B., Gregory, S.P. 2018. Comparison of heterotrophic bioleaching and ammonium sulfate ion exchange leaching of rare earth elements from a Madagascan ion-adsorption clay. Minerals, 8, 236.

Bloom, P.R. The kinetics of gibbsite dissolution in nitric acid. Soil Sci. Soc. Am. J., 1983, 47, 164–168.

Chakhmouradian, A.R., Wall, F. Rare earth elements: minerals, mines, magnets (and more). Elements, 2012, 8 (5): 333–340.

425 Chi, R.A., Zhou, Z., Xu, Z., Hu, Y., Zhu, G., Xu, S. Solution-chemistry analysis of ammonium
426 bicarbonate consumption in rare-earth-element precipitation. Metall. Materi. Trans. B 2003, 34
427 (5), 611–617.

428 Crawford, A. Geochemical modelling of environmental processes in rare earth element mining.
429 2019, PhD thesis, University of Leeds. [http://etheses.whiterose.ac.uk/id/eprint/23242]

430 Estrade, G., Marquis, E., Smith, M., Goodenough, K., Nason, P. REE concentration processes
431 in ion adsorption deposits: Evidence from the Ambohimirahavavy alkaline complex in
432 Madagascar, Ore Geol. Rev., 2019, 112, 103027.

433 Fernandes, A., Afonso, J.C., Dutra, A.J.B. Separation of nickel(II), cobalt(II) and lanthanides
434 from spent Ni-MH batteries by hydrochloric acid leaching, solvent extraction and precipitation.
435 Hydrometallurgy, 2013, 133, 37-43.

436 He, Z.Y., Zhang, Z.Y., Yu, J.X., Xu, Z.G., Chi, R.A. Process optimization of rare earth and
437 aluminum leaching from weathered crust elution-deposited rare earth ore with compound
438 ammonium salts. J. Rare Earths, 2016, 34, 413–419.

439 Josso, P., Roberts, S., Teagle, D.A.H., Pourret, O., Herrington, R., Albarran, C.P.L. Extraction
440 and separation of rare earth elements from hydrothermal metalliferous sediments. Minerals
441 Engineering, 2018, 118, 106-121.

442 Kanazawa, Y., Kamitani, M. Rare earth minerals and resources in the world. J. Alloys Compd,
443 2006, 408-412, 1339-1343.

444 Kasaini, H. Extraction of metals from metallic compounds. US patent application US
445 2015/035402.6 A1, 10th Dec 2015.

446 Kynicky, J., Smith, M.P., Xu, C. Diversity of rare earth deposits: The key example of China.
447 Elements, 2012, 8, 361-367.

448 Le Couteur, P.C. Geological Report on the Chambe Basin Area of Exclusive Prospecting
449 License EPL0325/11 Mulanje Massif, Southern Malawi, East Africa. 2011.

450 Lide, D.R. Ed. Physical Constants of Organic Compounds", in CRC Handbook of Chemistry
451 and Physics, 86th Edition, 2005, CRC Press, Boca Raton, FL, USA.

452 Martell, A.E. Smith, R.M., Motekaitis, R.J. NIST Critically Selected Stability Constants of Metal
453 Complexes, Database 46, Version 8, NIST, Gaithersburg, MD, 2004.

Meeussen, J.C.L., van der Sloot, H.A., Dijkstra, J.J., Kossen, D.S., 2009. Review of thermodynamic and adsorption databases. Cementitious Barriers Partnership Publication CBP-TR-2009-002.

Mentani, T., Ohmura, T., Watanabe, Y., Urabe, T. So-called ion-adsorption type REE deposits found in weathered crust of ilmenite-series granite in northern Vietnam. GSA Denver Annual Meeting. 2010.

Moldoveanu, G.A., Papangelakis, V.G. Recovery of rare earth elements adsorbed on clay minerals: I. Desorption mechanism. 2012, Hydrometallurgy 117–118, 71–78.

Moldoveanu, G.A., Papangelakis, V.G. Recovery of rare earth elements adsorbed on clay minerals: II. Leaching with ammonium sulfate. 2013, Hydrometallurgy 131–132, 158–166.

Moldoveanu, G.A., Papangelakis, V.G. Leaching of lanthanides from various weathered elution deposited ores. Can. Metall. Q. 2013b, 52, 257–264.

Moldoveanu, G.A., Papangelakis, V.G. An overview of rare-earth recovery by ion-exchange leaching from ion-adsorption clays of various origins. Min. Mag., 2016, 80, 63–76.

Padrones, J.T., Imai, A., Takahashi, R. Geochemical Behavior of Rare Earth Elements in Weathered Granitic Rocks in Northern Palawan, Philippines. Resour. Geol., 2017, 67, 231–253.

Parkhurst, D.L. Appelo, C.A.J. Description of input and examples for PHREEQC version 3—A computer program for speciation, batch-reaction, one-dimensional transport, and inverse geochemical calculations. US Geological Survey Techniques and Methods (Denver, CO) Book 6, Chapter A43, 2013. [Available at https://pubs.usgs.gov/tm/06/a43; accessed June 19, 2018].

Rocha, A., Schissel, D., Sprecher, A., de Tarso, P., & Goode, J. Process development for the Serra Verde weathered crust elution-deposited rare earth deposit in Brazil. Proceedings of the 52rd Conference of Metallurgists. 2013.

Sanematsu, K., Murakami, H., Watanabe, Y., Duangsurigna, S., Vilayhack, S. Enrichment of rare earth elements (REE) in the granitic rocks and their weathered crusts in central and southern Laos. Bull. Geol. Surv. Jpn., 2009, 60, 527–558.

SRK Exploration Services Ltd. A Competent Persons Report on the Tantalus Project, Northern Madagascar. 2013. [http://www.tre-ag.com/~/media/Files/T/Tantalus-Rare-

Earths/Attachments/pdf/2013_01_21_ES7520_SRKES_Tantalus%20CPR_Final_English.pdf ; Accessed 14th March 2019].

[Dataset] Stockdale, A., Banwart, S.A., SoS Minerals Madagascar ion adsorption deposits, inorganic leaching of rare earth elements. British Geological Survey - National Geoscience Data Centre. 2021. https://webapps.bgs.ac.uk/services/ngdc/accessions/index.html?#item163345

Stoltz, N.B. Geometallurgical investigations of ion adsorption clays. 2017. Thesis, Rheinisch-Westfälischen Technischen Hochschule Aachen.

Urabe, T., Tsugoshi, T. and Tanaka, M. Characterization of aluminum species with nitrate, perchlorate and sulfate ions in the positive and negative ion mode by electrospray ionization mass spectrometry. 2009, J. Mass Spectrom., 44, 193–202.

USGS (U.S. Geological Survey). Mineral commodity summaries, rare earths. January 2020. 2pp. [https://www.usgs.gov/centers/nmic/rare-earths-statistics-and-information; accessed 13th March 2020]

Vahidi, E., Navarro, J., Zhao, F. An initial life cycle assessment of rare earth oxides production from ion-adsorption clays. Resour. Conserv. Recy. 2016, 113, 1–11.

Weaver, B. Fractional Separation of Rare Earths by Oxalate Precipitation from Homogeneous Solution. Anal. Chem. 1954, 26, 479–480.

Wieland, E., Stumm, W. Dissolution kinetics of kaolinite in acidic aqueous solutions at 25°C. Geochim. Cosmochim. Acta, 1992, 56 (9), 3339–3355.

Xia, C. Direct oxalate precipitation for rare earth elements recovery. International patent application WO 2018/195642 A1, 1st Nov 2018.

Xiao, Y., Chen, Y., Feng, Z., Huang, X., Huang, L., Long, Z., Cui, D. Leaching characteristics of ion-adsorption type rare earths ore with magnesium sulfate Trans. Nonferrous Met. Soc. China, 2015, 25, 3784–3790.

Xiao, Y.F., Feng, Z.Y., Huang, X.W., Huang, L., Chen, Y.Y., Liu, X.S., Wang, L.S., Long, Z.Q. Recovery of rare earth from the ion-adsorption type rare earths ore: II. Compound leaching. Hydrometallurgy, 2016, 163**,** 83–90.

Xiao, Y.F., Feng, Z.Y., Hu, G.H., Huang, L., Huang, X.W. Chen, Y.Y., Long, Z.Q. Reduction leaching of rare earth from ion-adsorption type rare earths ore with ferrous sulfate, J. Rare Earths, 2016b, 34, 917–923.

515 Xiao, Y.F., Lai, F.G., Huang, L., Feng, Z.Y., Long, Z.Q. Reduction leaching of rare earth from
516 ion-adsorption type rare earths ore: II. Compound leaching. Hydrometallurgy, 2017, 173, 1–8.

517 Yang, X. Zhang, J. Recovery of rare earth from ion-adsorption rare earth ores with a
518 compound lixiviant. Sep. Purif. Technol. 2015, 142, 203–208.

519

Figures

Figure 1.

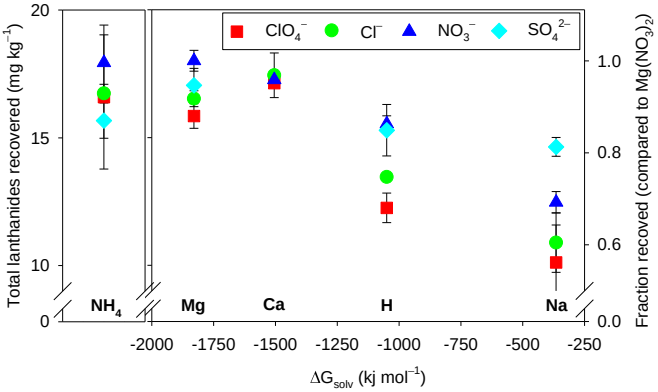

Figure 2.

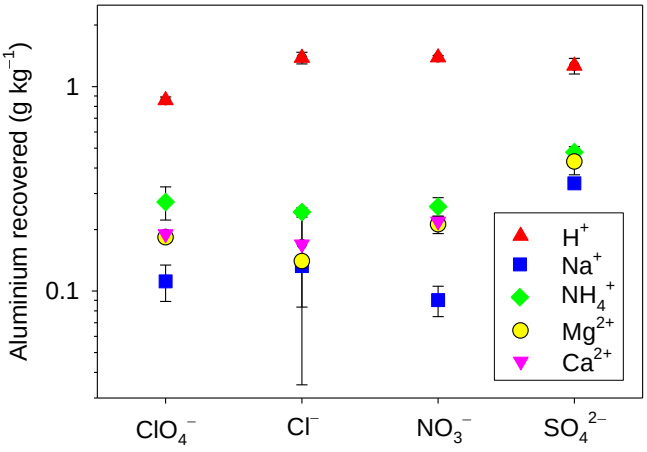

527 Figure 3.

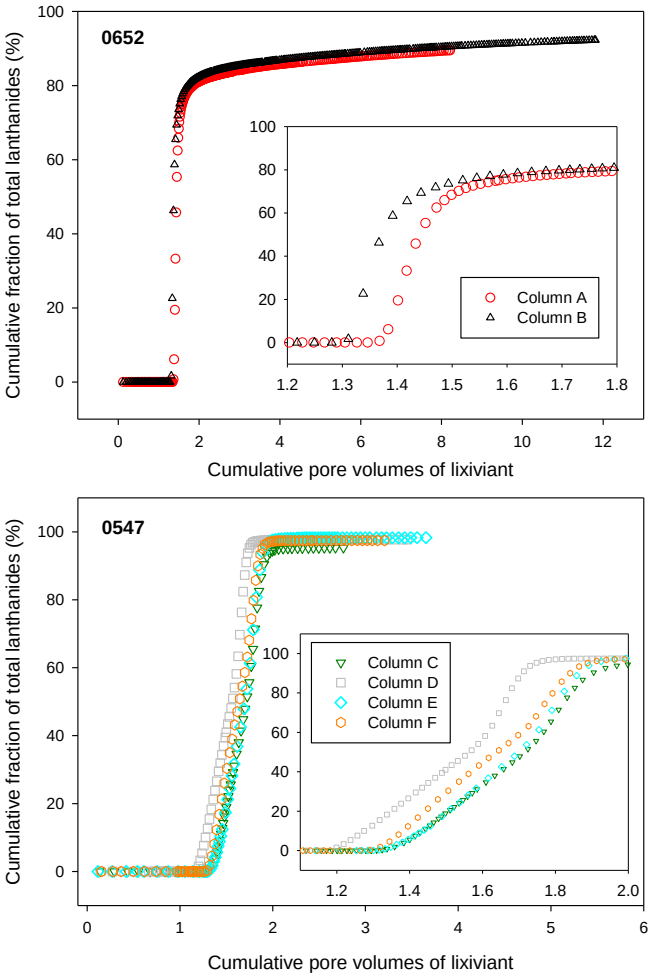

528

529

530 Figure 4.

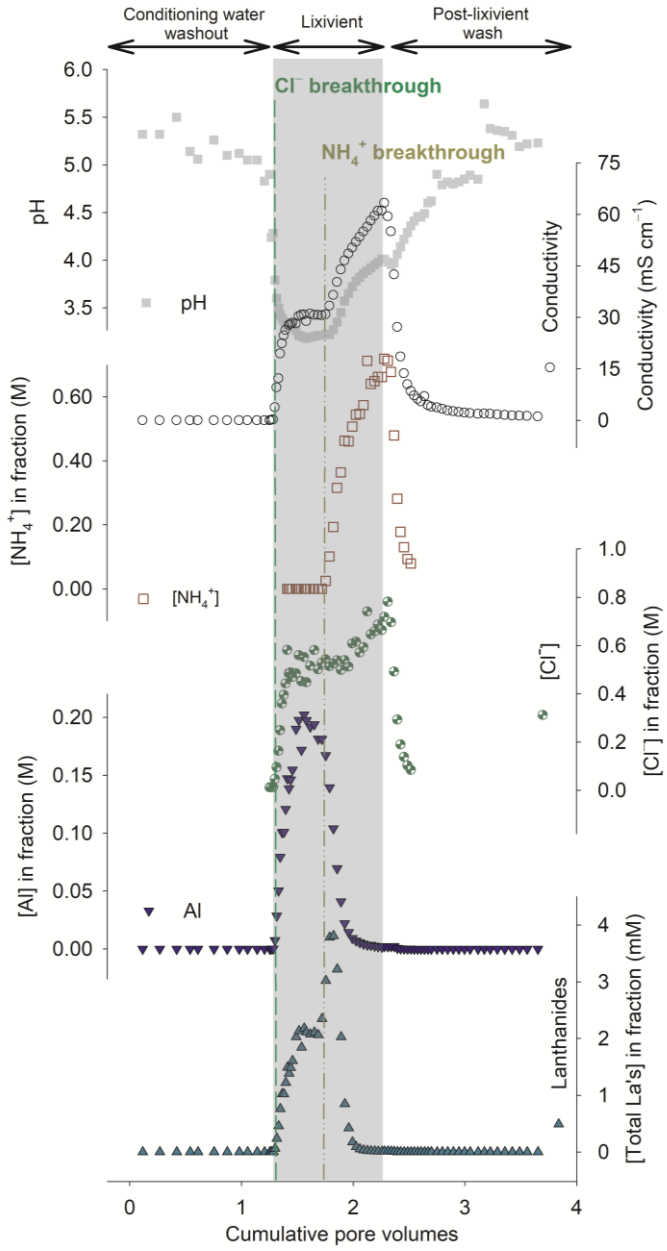

531

Figure Legends

Figure 1. Effect of lixiviant anions and cations on the extent of lanthanide leaching from an ion-adsorption soil in a batch experiment. Lixiviant cations are plotted against their solvation Gibbs free energies, except those for ammonium where data is not available so are plotted on an independent axis to the left of the main panel. Experimental conditions were a 1:1 solid:liquid ratio and a concentration of 1 M (0.5 M for salts containing divalent cations or anions). Error bars are two standard deviations from the mean of triplicate analysis.

Figure 2. Aluminium recovered from ion-adsorption soil using different lixiviant solutions. Experimental conditions were a 1:1 solid:liquid ratio and a concentration of 1 M (0.5 M for salts containing divalent cations or anions). Error bars are two standard deviations from the mean of triplicate analysis.

Figure 3. Total lanthanide recovery in samples 0652 and 0547 as a fraction of the total available from cation exchange leaching (column lixiviant flow and a final 1M $CaCl_2$ leach). The inset shows data zoomed at the breakthrough of the lixiviant at the column outflow. The equivalent data in molar concentration is shown in SI Figure S3.5.

Figure 4. Breakthrough curves for multiple analytes, for sample 0547 (column E). The breakthrough points for Cl and ammonia are annotated as vertical lines. The lixiviant was 1 M NH_4Cl (see Tables S2.2., S2.3. and S2.4. for other parameters). For columns C, D and F see SI Figure S3.7. Arrows indicate the solution being eluted. The conditioning fluid that is in equilibrium with the column before lixiviant injection is eluted first. This is followed by lixiviant breakthrough (not reaching the ion concentrations of the input lixiviant due to mixing in the columns and the low volume used). Then the lixiviant is washed out with the low ionic strength wash solution (MQ water).